Springer
Acta Mechanica Sinica
CrossMark click for updates
• RESEARCH PAPER •
Acta Mech. Sin., Vol. 39, ??? (2023)
https://doi.org/10.1007/s10409-023-???-?

Characteristic Resistance Change of No-insulation REBCO Pancake Coils by Deformation

So Noguchi[1*]

[1]*Hokkaido University, Kita 14 Nishi 9, Kita-ku Sapporo, 060-0814, Japan*

Received ???; accepted ???; published online ???

In recent years, the deformation of rare-earth barium copper oxide (REBCO) pancake coils for high magnetic field generations attracts attention. Several screening current simulation considering coil deformation shows a possibility that coil deformation affected screening current distribution. Screening currents would produce strong electromagnetic forces to mechanically damage REBCO pancake coils. Whereas, coil deformation also possibly affects the contact resistances of no-insulation (NI) REBCO pancake coils often called the "characteristic resistances." The NI characteristic resistances are an important factor of the stability of NI REBCO pancake coil. Therefore, it is necessary to investigate the NI contact resistances as the coil shape deforms. As the result, the NI characteristic resistance change during an external field charging and an NI coil charging is shown in this paper.

High field magnet, No-insulation winding technique, REBCO pancake coil, Characteristic resistance

Citation: S. Noguchi, Characteristic Resistance Change of No-insulation REBCO Pancake Coils by Deformation, Acta Mech. Sin. **39**, ??? (2023), https://doi.org/10.1007/s10409-023-???-?

1. Introduction

High magnetic fields beyond 20 T are strongly desired for various applications; compact fusion reactor [1-3], medical use accelerator [4, 5], nuclear magnetic resonance (NMR) [6-10], and so on. Since an insert rare-earth barium copper oxide (REBCO) magnet with a no-insulation (NI) winding technique [11] successfully generated 14.4 T inside 31.1 T (45.5 T in total) [12], REBCO coated conductors are widely recognized as a suitable superconducting wire to generate a high magnetic field beyond 20 T with a compact space.

The NI winding technique enhancing the thermal stability can protect REBCO pancake coils from burning-out, mechanical damage, and critical-current degradation. The NI REBCO pancake coils are not insulated between turns, so that the operating currents can be prevented from flowing into normal-state zones. That is, the operating currents are carried in the radial direction around the normal-state zones through turn-to-turn contact resistances called the "characteristic resistances." The characteristic resistances characterize the thermal stability of NI REBCO pancake coils, and it was investigated on some papers [13-16].

In the previous paper [13], the relation of temperature rise and charging delay to the characteristic resistance was discussed. Fig. 1 shows the temperature rise at the appearance of local normal zone. As the characteristic resistance increases, the temperature rise increases. A current avoiding the local normal zone carries onto the radial direction through turn-to-turn surfaces with contact resistances. High contact resistances increases the coil temperature. A large temperature rise is followed by coil's burning-out. That is, high characteristic resistances bring NI REBCO pancake coils to thermal instability. Meanwhile, a low characteristic resistance results in another problem. A leakage current in the coil-radial direction appears when charging an NI REBCO coil. That phenomenon is known as "charging delay." Low characteristic resistances bring NI REBCO pancake coils to electromag-

*Corresponding author. E-mail address: noguchi@ssi.ist.hokudai.ac.jp (So Noguchi)
Executive Editor: ???

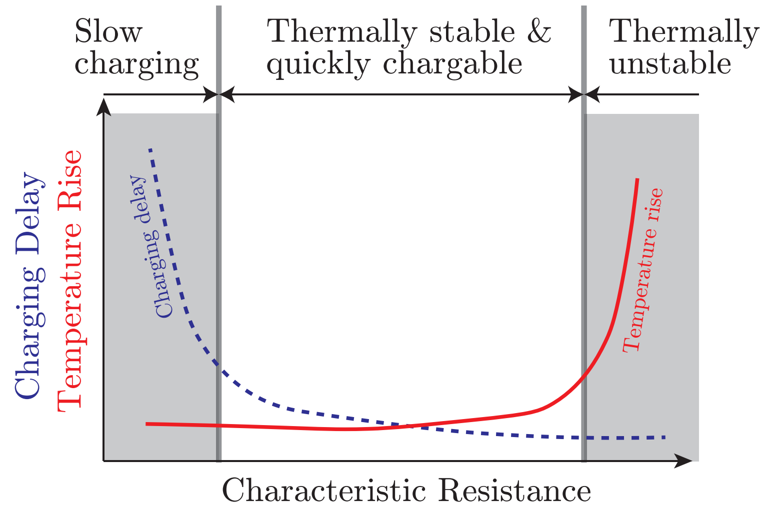

Figure 1 Temperature rise (red solid line) of NI REBCO pancake coil when a local normal-state transition occurs. In the region of high characteristic resistance, high temperature rise deteriorates the coil stability, occasionally resulting in burning-out. Charging delay τ (blue broken line) defined as $\tau = L/R_{\mathrm{ct\_all}}$, where L and $R_{\mathrm{ct\_all}}$ are respectively the coil inductance and the characteristic resistance, when charging NI REBCO pancake coil. In the region of low characteristic resistance, long charging delay is observed. In the region of middle characteristic resistance, thermal stability and quick charging are obtained as the good performance for NI REBCO pancake coils [13].

netic performance deterioration. A characteristic resistance suitable to the coil inductance is required as shown in Fig. 1, to achieve both high thermal stability and no charging delay. Consequently, the characteristic resistance is a very important factor of NI REBCO coils.

In recent years, mechanical damages on REBCO pancake coils have attracted attentions. Strong electromagnetic forces due to high fields and large currents work to REBCO pancake coils. Screening currents cause additional strong forces to rotate REBCO coated conductors. It results in complicated current behaviors as well as plastic deformations followed by critical-current deterioration [17-20].

According to my deformation simulation results presented before [20,21], some gaps are created due to the REBCO tape rotation. Such gaps, i.e. non-contact tapes each other, increases the characteristic resistances. However, the characteristic resistance is commonly regarded as constant. In this paper, I investigated the characteristic resistance change during the charging of NI REBCO pancake coil by numerical simulation considering both the current and deformation behaviors. A large increase of the characteristic resistance has a possibility to deteriorate the thermal stability of NI REBCO pancake coil.

2. Simulation Method

To investigate the characteristic resistances of NI REBCO pancake coil, the current and deformation behaviors are simulated with a partial element equivalent circuit (PEEC) model, also called the "network model" [22,23], and an elastic finite element method (FEM). The characteristic resistances are affected by the contact area between turns of REBCO coated conductors.

2.1 PEEC model

The PEEC model is employed as an electromagnetic simulation method. An NI REBCO pancake coil is expressed with self-/mutual inductances L, azimuthal-directional REBCO resistances R_θ, transverse-directional REBCO resistances R_{t}. and radial-directional characteristic resistances R_{ct}, as shown in Fig. 2. This complicated PEEC model proposed in [24] can represent the screening currents in REBCO coated conductors.

The total characteristic resistance in an NI REBCO pancake coils, $R_{\mathrm{ct\_all}}$, is derived from [25]

$$R_{\mathrm{ct\_all}} = \sum_{i=1}^{N_{\mathrm{t}}-1} \frac{\rho_{\mathrm{ct}}}{2\pi r_i w_{\mathrm{d}}} \tag{1}$$

where N_{t}, ρ_{ct}, r_i and w_{d} are the total number of turns, the average turn-to-turn contact resistance in units of $\Omega \cdot \mathrm{m}^2$, the radius of ith turn, and the REBCO tape width, respectively.

Meanwhile, a local contact resistance R_{ct} used in the PEEC model is given by

$$R_{\mathrm{ct}} = \frac{\rho_{\mathrm{ct}}}{S_{\mathrm{ct}}} \tag{2}$$

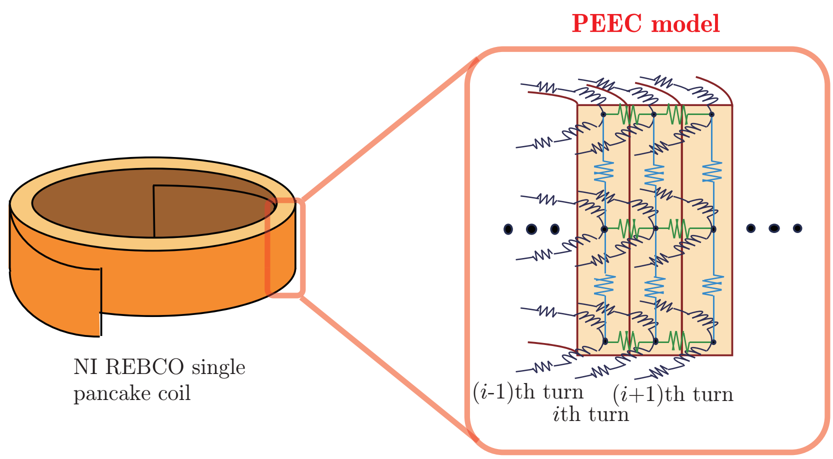

Figure 2 Partial element equivalent circuit (PEEC) model representing an NI REBCO pancake coil. Black components show azimuthal inductances and REBCO resistances, blue ones tape-transverse REBCO resistances. Green resistances are local NI characteristic resistances.

where S_{ct} is the local contact area of turn-to-turn. To feed the deformation FEA results back to the PEEC model, if a contact between turns is lost, the local contact area S_{ct} is set to a large value. Actually, although the local contact resistance R_{ct} at the lost contact should be infinity, it is set to a value large enough to be regarded as an insulation for numerical simulation.

2.2 Deformation FEA

The coil deformation is obtained with 2-dimensional finite element analysis (FEA) on the coil-cross-sectional plane by solving the following equations:

$$\frac{\partial \sigma_{\mathrm{r}}}{\partial r}+\frac{\partial \sigma_{\mathrm{rz}}}{\partial z}+\frac{\sigma_{\mathrm{r}}-\sigma_{\mathrm{z}}}{r}+J_{\theta} B_{\mathrm{z}}=\rho \frac{\partial^2 u_{\mathrm{r}}}{\partial t^2} \tag{3}$$

$$\frac{\partial \sigma_{\mathrm{rz}}}{\partial r}+\frac{\partial \sigma_{\mathrm{z}}}{\partial z}+\frac{\sigma_{\mathrm{rz}}}{r}-J_{\mathrm{z}} B_{\mathrm{r}}=\rho \frac{\partial^2 u_{\mathrm{z}}}{\partial t^2} \tag{4}$$

where σ_{r}, σ_{z}, σ_{rz}, ρ, u_{r}, u_{z}, J_θ, J_{z}, B_{r}, and B_{z} are respectively the radial, the hoop, and the share stresses, the mass density, the radial and the axial displacements, the azimuthal and the axial current densities, and the radial and the axial magnetic flux densities. The constitutive equations (Hooke's law) are given as

$$\varepsilon_r=\frac{1}{E_r}\sigma_r-\frac{\nu_{\theta r}}{E_\theta}\sigma_\theta-\frac{\nu_{zr}}{E_z}\sigma_z=\frac{\partial u_r}{\partial r} \tag{5}$$

$$\varepsilon_\theta=-\frac{\nu_{r\theta}}{E_r}\sigma_r+\frac{1}{E_\theta}\sigma_\theta-\frac{\nu_{z\theta}}{E_z}\sigma_z=\frac{u_r}{r} \tag{6}$$

$$\varepsilon_z=-\frac{\nu_{rz}}{E_r}\sigma_r-\frac{\nu_{\theta z}}{E_\theta}\sigma_\theta+\frac{1}{E_z}\sigma_z=\frac{\partial u_z}{z} \tag{7}$$

where $\varepsilon_{\{r,\theta,z\}}$, $E_{\{r,\theta,z\}}$, and ν_{12} are, respectively, the strains and the Young's moduli in the radial, azimuthal, and axial directions, and the Poisson's ratio ($\nu_{12}=-\varepsilon_2/\varepsilon_1$). The Young's moduli and the Poisson's ratio are treated as a single composite material considering the layer structure by the rule of mixture [18], because the REBCO tape has some layers consisting of REBCO superconductor, Hastelloy substrate, silver layer, and so on [26]. Here, the current densities and the magnetic flux densities computed with the PEEC model are substituted into (3) and (4).

To consider the contacts between turns, the Karush-Kuhn-Tucker (KKT) condition [27] is implemented into the deformation FEA.

$$\frac{\partial W(u)}{\partial u}+\mu\frac{\partial G(u)}{\partial u}=0 \tag{8}$$

$$\mu \geq 0 \tag{9}$$

$$\mu G(\mu)=0 \tag{10}$$

where W, G, u and μ are the objective function, which corresponds to the governing equations of the deformation FEA, the constraint condition function of the distance between the adjacent turns, the displacement, and the penalty parameter, respectively. The KKT equations are solved with the Newton-Raphson method.

2.3 Characteristic Resistance Change

In this paper, I propose the change of the characteristic resistance R_{ct} in (2) according to the coil deformation computed from (3) and (4). The local contact area S_{ct} is obtained as shown in Fig. 3. As shown in Figs. 3(a) and (b), when the windings are contacted, the local contact resistance R_{ct}

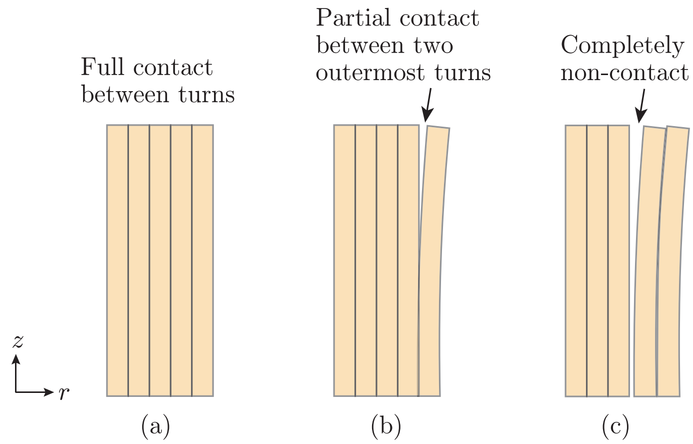

Figure 3 Conceptual relation between coil deformation and characteristic resistance. (a) realistic turn-to-turn contact condition, (b) partial contact between 4th and 5th turn due to deformed 5th-turn REBCO coated conductor resulting in increase in characteristic resistance, and (c) no contact between 3rd and 4th turns causing infinite characteristic resistance.

can ordinarily be obtained from the contact REBCO tape surface area. Whereas, when the turns are not contacted like Figs. 3(c), the local contact resistance R_{ct} is infinite ($R_{\text{ct}} = \infty$). The local contact resistances R_{ct} obtained according to the coil deformation are fed back to the Kirchhoff's voltage equation constructed in the PEEC model.

3. Characteristic Resistance Behaviors

3.1 Simulation Conditions

As a first fundamental investigation, I have simulated an insert HTS coil whose specifications are listed in Table 1. Fig. 4 shows the schematic cross-sectional view of the simulated NI REBCO pancake coil with an outsert copper magnet. The insert HTS coil is located at 25 cm above the outsert magnet center to purposely increase the screening currents in the REBCO coated conductor. Large screening currents induce large coil deformation, and it would create some large local gaps between turns. Table 1 also lists the specifications of outsert copper magnet to generate an external magnetic field B_{ex}.

The operating pattern is as follows: (1) the outsert magnet charges to $B_{\text{ex}} = 20\,\text{T}$ at a speed of $0.01\,\text{T}\cdot\text{s}^{-1}$, (2) it keeps charging up to 30 T at $0.005\,\text{T}\cdot\text{s}^{-1}$, and then (3) the operating current I_{op} of insert NI REBCO pancake coil increases to 400 A at $1\,\text{A}\cdot\text{s}^{-1}$.

3.2 Simulation Result

Fig. 5 illustrates the deformed REBCO coil shapes with the current density maps at different times. At the initial state of Fig. 5(a) ($t = 0$ s), before the deformation of NI REBCO coil, the initial characteristic resistance is 1.8 µΩ derived from (1) with $\rho_{\text{ct}} = 7\ \mu\Omega\cdot\text{cm}^2$. During charging the outsert magnet, since the screening current is induced, a gap appears on the upper contact surface between 4th and 5th turns as shown in Figs. 5(b) and (c). The electrical contact is lost on this surface, and the local contact resistance between 4th and 5th turns increases from 0.5 to 0.8 µΩ. Consequently, the total characteristic resistance is $R_{\text{ct\_all}} = 2.2\ \mu\Omega$.

Fig. 5(d) shows the current density map with deformation at $t = 3000$ s. At this moment, there are gaps between 1st-2nd and 2nd-3rd turns. As the time elapses, the gaps moves from the outer to the inner turn-to-turn. The total characteristic resistance is $R_{\text{ct\_all}} = 2.4\ \mu\Omega$ at $t = 3000$ s.

At the end of charging the external field ($t = 4000$ s, $B_{\text{ex}} = 30$ T), $R_{\text{ct\_all}}$ decreases back to 1.9 µΩ. As shown in Fig. 5(e), since the NI REBCO pancake coil finishes to be expanded, the turn-to-turn contact area is likely back to the initial state.

At $t = 4135$ s during charing the operating current of NI REBCO pancake coil, the total contact resistance is 6.5 µΩ at maximum of this simulation. As we can see in Fig. 5(f), the winding partly loses contact every turn-to-turn. When completing the charging, since no gap appears, the total contact resistance $R_{\text{ct\_all}}$ is 1.9 µΩ again.

Finally, Fig. 6 shows the total contact resistance time-transition.

4. Conclusion

In recent years, some simulation results of REBCO coil deformation have been reported, and the deformation affects the screening current behaviors. In this paper, the effects of the coil deformation on the characteristic resistance of NI RE-

Table 1 Specifications of insert NI REBCO pancake coil and outsert copper magnet

NI REBCO pancake coil		***Outsert copper magnet***	
Number of pancake coils	1	Inner diameter (cm)	16.8
Inner diameter (mm)	120	Magnet thickness (cm)	18.6
REBCO tape width (mm)	4	Magnet height (cm)	64
REBCO tape thickness (mm)	0.1	Maximum field (T)	30
Number of turns	5		
Avg. characteristic resistivity ρ_{ct} ($\mu\Omega \cdot cm^2$)	7		
Operating temperature (K)	4.2		

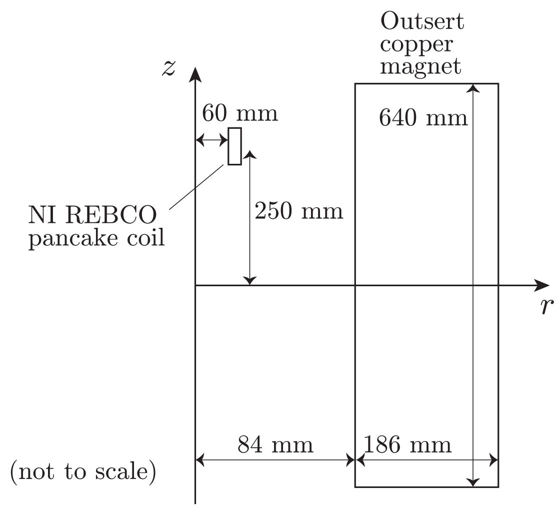

Figure 4 Cross section of NI REBCO pancake coil and outert copper magnet (not to scale). NI REBCO pancake coil is place off-center above 250mm.

BCO pancake coils have been investigated on numerical simulation. The current and deformation behaviors are simulated with the partial element equivalent circuit (PEEC) model and the deformation finite element method (FEM).

In the simulation, the increase of the external magnetic field is followed by the charging of the insert NI REBCO pancake coil. At the beginning of the external field excitation, the NI characteristic resistance increases due to air gap appearance. After the characteristic resistance once decreases back to the initial value, it increases again. At final, completing the expansion of NI REBCO pancake coil, the characteristic resistance is, once again, back to the initial one.

In the near future, it is necessary to investigate the thermal stability of NI REBCO pancake coil while the characteristic resistance changes at coil charging.

1 P. Bruzzone, et al., High temperature superconductors for fusion magnets, Nucl. Fusion **58**, 103001 (2018).
2 A. J. Creely, et al., Overview of the SPARC tokamak, J. Plasma Phys. **86**, 865860502 (2010).
3 Z. S. Hartwig, et al., The SPARC toroidal field model coil program, submitted.
4 J. Nugteren, et al., Toward REBCO 20 T+ dipoles for accelerators, IEEE Trans. Appl. Supercond. **28**, 4008509 (2018).
5 S. Takayama, et al., Development of an HTS accelerator magnet with REBCO coils for test at HIMAC beam line, IEEE Trans. Appl. Supercond. **29**, 4004205 (2019).
6 Y. Iwasa, et al., A high-resolution 1.3-GHz/54-mm LTS/HTS NMR magnet, IEEE Trans. Appl. Supercond. **29**, 4300205 (2019).
7 Y. Yanagisawa, et al., Development of a persistent-mode NMR magnet with superconducting joints between high-temperature superconductors, Supercond. Sci. Tech. **34**, 115006 (2021).
8 S. Iguchi, et al., Advanced field shimming technology to reduce the influence of a screening current in a REBCO coil for a high-resolution NMR magnet, Supercond. Sci. Tech. **29**, 045013 (2016).
9 D. Park, J. Bascuñán, Y. Li, W. Lee, Y. Choi, and Y. Iwasa, Design overview of the MIT 1.3-GHz LTS/HTS NMR magnet with a new REBCO insert, IEEE Trans. Appl. Supercond. **31**, 4300206 (2021).
10 K. Naito, et al., Analyses of deformation due to screening-current-induced force in layer-wound REBCO insert coil for 1.3-GHz LTS/HTS NMR, IEEE Trans. Appl. Supercond. **33**, 4300805 (2023).
11 S. Hahn, D. K. Park, J. Bascuñán, and Y. Iwasa, HTS pancake coils without turn-to-turn insulation, IEEE Trans. Appl. Supercond. **21**, 1592–1595 (2011).
12 S. Hahn, et al., 45.5-tesla direct-current magnetic field generated with a high-temperature superconducting magnet, Nature **570**, 496–499 (2019).
13 S. Noguchi, S. Hahn, A. Ishiyama, and Y. Iwasa, A simple protection

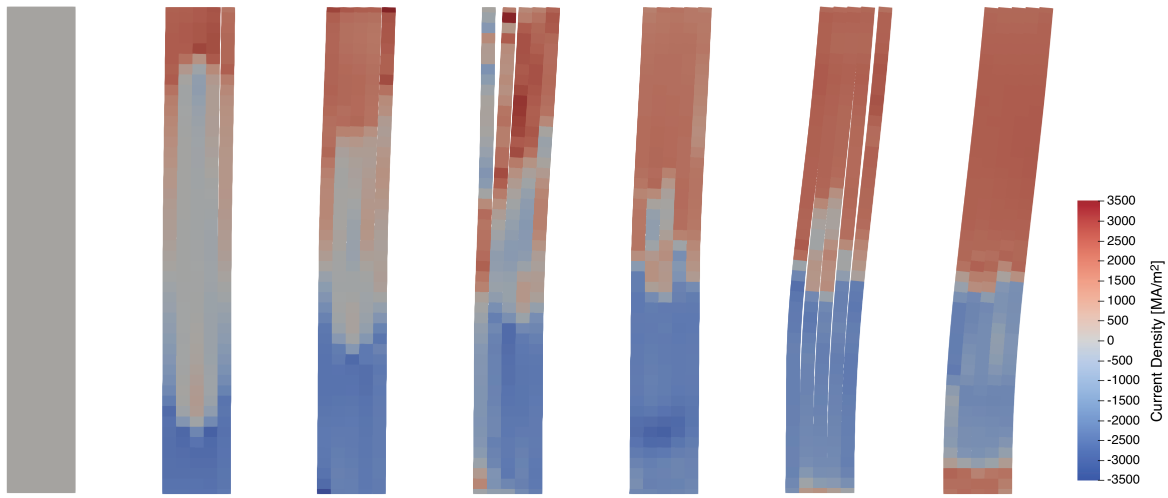

Figure 5 Deformed coil shapes with current density distributions at $t = 0, 1000, 2000, 3000, 4000, 4135$, and 4400 s. Coils of (b), (c), (d) and (f) have some gaps between turns increasing local characteristic resistances.

evaluation method for no-insulation REBCO pancake coils during local normal-state transition, Supercond. Sci. Tech. **32**, 045001 (2019).

14 H. Kobayashi, Y. Nakada, H. Saotome, D. Miyagi, Y. Nagasahi, and M. Tsuda, Numerical evaluation on current behavior of no-insulation coils with parallel HTS tapes, IEEE Trans. Appl. Supercond. **33**, 4601606 (2023).

15 P. Duan, et al., A numerical method for transient thermal analysis of no-insulation REBCO pancake coils with several resistive joints, IEEE Trans. Appl. Supercond. **33**, 4603410 (2023).

16 J. Choi, et al., Thermal analysis of leakage currents of no-insulation HTS racetrack coils using a three-dimensional turn-distributed equivalent circuit FEA model, IEEE Trans. Appl. Supercond. **33**, 5201106 (2023).

17 D. Kolb-Bond, M. Bird, I. R. Dixon, and T. Painter, Screening current rotation effects: SCIF and strain in REBCO magnets, Supercond. Sci. Tech. **34**, 095004 (2021).

18 H. Ueda et al., Numerical evaluation of the deformation of REBCO pancake coil, considering winding tension, thermal stress, and screening-current-induced stress, Supercond. Sci. Tech. **34**, 024003 (2021).

19 H. Ueda et al., Deformation analysis of no-insulation REBCO coils considering turn-to-turn contact configuration, IEEE Trans. Appl. Supercond. **32**, 4604205 (2022).

20 S. Noguchi, T. Mato, K. Kim, and S. Hahn, Electromagnetic behavior simulation of REBCO pancake coils considering REBCO tape rotation under high magnetic field, IEEE Trans. Appl. Supercond. **33**, 4300405 (2023).

21 K. Kodaka and S. Noguchi, Stress and deformation analysis of REBCO pancake coils with individual turn movement, IEEE Trans. Appl. Supercond. **33**, 4600305 (2023).

22 W. D. Markiewicz, J. J. Jaroszynski, D. V. Abraimov, R. E. Joyner, and A. Khan, Quench analysis of pancake wound REBCO coils with low resistance between turns, Supercond. Sci. Technol. **29**, 025001 (2016).

23 Y. Wang, W. K. Chan, and J. Schwartz, Self-protection mechanism in no-insulation (RE)$Ba_2Cu_3O_x$ high temperature superconductor pancake coils, Supercond. Sci. Technol. **29**, 045007 (2016).

24 S. Noguchi and S. Hahn, A newly developed screening current simulation method for REBCO pancake coils based on extension of PEEC model, Supercond. Sci. Tech. **35**, 044005 (2022).

25 X. Wang et al., Turn-to-turn contact characteristics for an equivalent circuit model of no-insulation ReBCO pancake coil, Supercond. Sci. Tech. **26**, 035012 (2013).

26 https://www.superpower-inc.com/specification.aspx (2023).

27 H. W. Kuhn and A. W. Tucker, "Nonlinear programming," in Proc. 2nd Berkeley Symp. Math. Statics Probability, pp. 481–492 (1951).

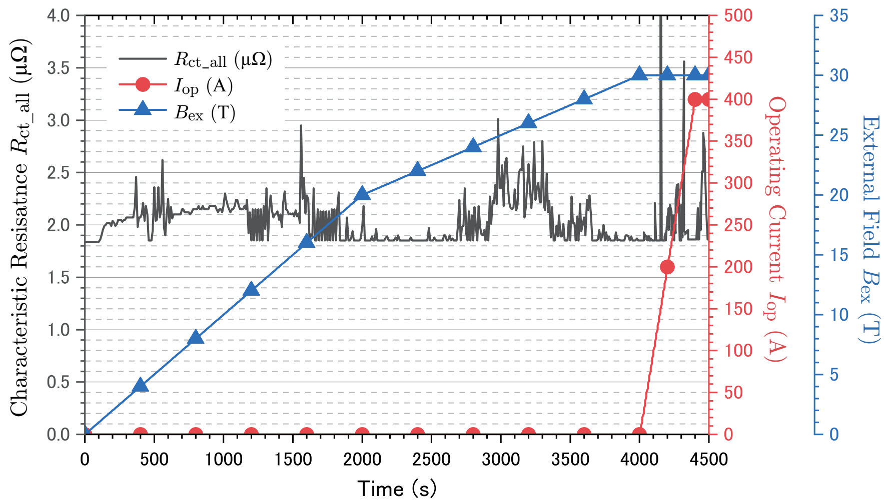

Figure 6 Characteristic resistance as a function of time. $R_{\mathrm{ct\_all}}$, I_{op}, and B_{ex} mean the total characteristic resistance of 5-turn NI REBCO pancake coil, the operating current, and the external field generated by the outsert magnet, respectively.